

**EphA4-dependent axon retraction and midline localization of Ephrin-B3 are disrupted in the spinal cord of mice lacking mDia1 and mDia3 in combination**

*Abbreviated title: Roles of mDia's in axon path finding*

Yosuke Toyoda,<sup>1†</sup> Ryota Shinohara,<sup>1†</sup> Dean Thumkeo,<sup>1†</sup> Hiroshi Kamijo,<sup>1</sup> Hiroshi Nishimaru,<sup>2</sup> Hiroyuki Hioki,<sup>3</sup> Takeshi Kaneko,<sup>3</sup> Toshimasa Ishizaki,<sup>1</sup> Tomoyuki Furuyashiki,<sup>1,4</sup> and Shuh Narumiya<sup>1,4\*</sup>

<sup>1</sup>Department of Pharmacology, Kyoto University Graduate School of Medicine, Yoshida-konoe-cho, Kyoto 606-8501, Japan

<sup>2</sup>Graduate School of Comprehensive Human Sciences, University of Tsukuba, 1-1-1 Tennodai, Tsukuba, Ibaraki 305-8577, Japan

<sup>3</sup>Department of Morphological Brain Science, Kyoto University Graduate School of Medicine, Yoshida-konoe-cho, Sakyo-ku, Kyoto 606-8501, Japan

<sup>4</sup>CREST, JST, 7 Gobancho, Chiyoda-ku, Tokyo 102-0076, Japan

<sup>†</sup>These authors equally contributed to this work.

\*Correspondence should be addressed to: Shuh Narumiya, M.D.,Ph.D., Department of Pharmacology, Kyoto University Graduate School of Medicine, Yoshida-konoe-cho, Sakyo-ku, Kyoto, 606-8501, Japan. TEL +81-75-753-4392, FAX +81-75-753-4693, Email snaru@mfour.med.kyoto-u.ac.jp

Keywords: Rho, axon guidance, growth cone, left-right limb coordination

This article has been published as an Original Article in *Genes to Cells* (18(10): 873-885, 2013; doi: 10.1111/gtc.12081). The publishing pdf version of this article and supplementary movies can be downloaded from the following website:

<http://onlinelibrary.wiley.com/doi/10.1111/gtc.12081/abstract>

**Abstract**

mDia is an actin nucleator and polymerization factor regulated by the small GTPase Rho and consists of three isoforms. Here, we found that mice lacking mDia1 and mDia3, two isoforms expressed in the brain, in combination (mDia-DKO mice) exhibit impaired left-right limb coordination during locomotion, and aberrant midline crossing of axons of corticospinal neurons and spinal cord interneurons. Given that mice lacking Ephrin-B3-EphA4 signaling exhibit the similar impairment in locomotion, we examined whether mDia is involved in Ephrin-B3-EphA4 signaling for axon repulsion. In primary cultured neurons, the mDia deficiency impairs growth cone collapse and axon retraction induced by chemo-repellants including EphA ligands. In mDia-DKO mice, the Ephrin-B3-expressing midline structure in the spinal cord is disrupted, and axons aberrantly cross the spinal cord midline preferentially through the region devoid of Ephrin-B3. Therefore, mDia plays multiple roles in the proper formation of the neural network in vivo.

## Introduction

For proper formation of neuronal networks, extracellular guidance cues either attract or repel axons of certain types of neurons at genetically determined locations in the brain (Kolodkin & Tessier-Lavigne 2011). Axons sense extracellular cues at their growing tips called the growth cone, and reorganize the cytoskeleton to steer themselves to appropriate directions.

The small GTPase Rho is critical for actin reorganization in various cell types, and mediates axon repulsion induced by several repulsive cues (Hall & Lalli 2010). Rho acts at least two effector molecules, ROCK and mDia, and induces actomyosin stress fibers in cultured fibroblasts (Narumiya *et al.* 2009). ROCK is a Rho-associated kinase that induces phosphorylation of myosin light chain and regulates myosin-based contractility. mDia is a formin family protein, and upon being activated by Rho, catalyzes actin nucleation and polymerization to produce long straight actin filaments (Higashida *et al.* 2004). Of these Rho effectors, ROCK has been established as a mediator of axon retraction (Hirose *et al.* 1998; Bito *et al.* 2000). Notably, inhibitors for Rho and ROCK abolish axon repulsion induced by ephrins and semaphorins in primary cultured neurons (Wahl *et al.* 2000; Shamah *et al.* 2001; Swiercz *et al.* 2002; Cheng *et al.* 2003; Gallo 2006). These findings have led to an idea and preclinical attempts to employ ROCK inhibitors for axon regeneration after nerve injury (Kubo *et al.* 2007). Thus, injection of ROCK inhibitors or genetic deletion of ROCK-II facilitates axon sprouting and functional recovery after spinal cord injury in rodents (Fournier *et al.* 2003; Chan *et al.* 2005; Duffy *et al.* 2009).

In contrast, a role for mDia in axon retraction remains unknown. Previous studies demonstrated that mDia mediates axon elongation in response to SDF-1 $\alpha$  in the primary

culture of cerebellar granule cells and cerebral cortical neurons (Arakawa *et al.* 2003; Ohshima *et al.* 2008). Thus, mDia mediates actions apparently opposite to ROCK in neuronal morphogenesis in some *in vitro* situations. However, whether mDia functions physiologically in axon elongation or retraction *in vivo*, and if so, how it functions in neural development remain unknown.

Among three mDia isoforms, mDia1 and mDia3 are expressed in the mouse brain during and after development (Shinohara *et al.* 2012). We therefore generated mice lacking mDia1 and mDia3 (Sakata *et al.* 2007; Shinohara *et al.* 2012). Since mice lacking either of these two isoforms alone did not have apparent abnormality, we generated mice lacking mDia1 and mDia3 in combination (mDia-DKO) by crossing mDia1<sup>+/-</sup>;mDia3<sup>null</sup> pairs. As we recently reported, these mice exhibit several abnormalities in neural development. First, mDia deficiency disrupts the integrity of apical surface of the neuroepithelium of developing brain, and this deficit appears to cause periventricular dysplasia, which eventually leads to hydrocephalus (Thumkeo *et al.* 2011). Second, mDia-DKO mice show impairment in tangential migration of olfactory and cortical inhibitory interneuron precursors, while radial migration of cortical excitatory neurons is intact (Shinohara *et al.* 2012). Besides these findings, mDia-DKO mice exhibit abnormal gait pattern during locomotion, suggesting an abnormal formation of the neural network. Here we have examined how mDia functions in axon guidance *in vivo* and *in vitro*.



## Results

### **Mice lacking mDia1 and mDia3 in combination exhibit impaired left-right limb alternation during locomotion**

We noticed rabbit-like hopping gait of mDia-DKO mice first in their home cages. We therefore examined their gait pattern by recording footprints of mice of various mDia genotypes during locomotion. Whereas wild-type mice showed a normal alternating pattern of left and right hindlimb movement during locomotion, mDia-DKO mice showed abnormal synchrony of left and right hindlimb movement (Fig. 1A; Movie S1). Abnormal left-right synchrony was also observed in forelimb movement of mDia-DKO mice (data not shown). For quantitative analysis, we determined the ratio of the distance between adjacent footprints of left and right hindlimbs ('B') and the distance between adjacent footprints of the same hindlimb ('A') (Fig. 1B). The B/A ratio indicates the degree of left-right hindlimb alternation, such that left-right limb alternation and synchrony correspond to 0.5 and 0.0, respectively. In wild-type mice, the B/A ratio was  $0.48 \pm 0.03$ , indicating normal left-right hindlimb alternation (Fig. 1B). In contrast, this ratio was significantly reduced to  $0.10 \pm 0.01$  in mDia-DKO mice (Fig. 1B). These data showed that the loss of mDia1 and mDia3 in combination leads to defective left-right limb coordination during locomotion. Such a deficit was absent in either mDia1-KO ( $mDia1^{-/-};mDia3^{+/Y}$ ), mDia3-KO ( $mDia1^{+/+};mDia3^{null}$ ) or mDia1-heterozygous, mDia3-KO ( $mDia1^{+/-};mDia3^{null}$ ) mice (Fig. 1A) as confirmed by the B/A ratio (Fig. 1B). Therefore, mDia1 and mDia3 play redundant roles in formation of neuronal circuits underlying gait control.

### **mDia-DKO mice exhibit aberrant midline crossing of axons of spinal cord**

### **interneurons and corticospinal neurons**

Several knockout mice lacking molecules involved in axon guidance, such as Ephrin-B3 and EphA4, have similar synchronous pattern of the left-right limbs during locomotion (Kullander *et al.* 2001; Kullander *et al.* 2003; Wegmeyer *et al.* 2007). Since those mice exhibited aberrant midline crossing of axons of spinal cord interneurons and corticospinal neurons, we examined whether similar anatomical abnormalities exist in mDia-DKO mice in the following manners. First, we examined axonal projections of spinal cord interneurons in mDia-DKO mice by unilateral injection of RDA to the ventral side of the spinal cord of wild-type and mDia-DKO neonates. Wild-type mice showed anterogradely labeled axons contralateral to the injection side only at the most ventral region of the spinal cord (upper panels in Fig. 2A, dashed circle). This is consistent with the presence of commissural axons of spinal cord interneurons, as previously reported (Kiehn & Butt 2003). Similar ventral commissural fibers were also observed in the spinal cord of mDia-DKO mice (lower panels in Fig. 2A, dashed circle). However, in addition to these axons, a larger number of anterogradely labeled axons projected to the side contralateral to the injection in mDia-DKO mice (Fig. 2A). Such aberrant midline crossing of axons in mDia-DKO mice was observed dorsal to the location of normal commissural axons in both genotypes (Fig. 2A, arrowheads). The dorso-ventral distribution of RDA-labeled axons that crossed the midline significantly differed between wild-type and mDia-DKO mice (Fig. 2A, B). These findings indicate that mDia deficiency causes aberrant midline crossing of spinal cord interneurons.

We next examined whether aberrant midline re-crossing of corticospinal tract occurs in mDia-DKO mice. To this end, we unilaterally injected BDA into the primary motor cortex of adult wild-type and mDia-DKO mice and examined the projection of

these axons in the pyramidal decussation and in the spinal cord (Fig. 3A). In both wild-type and mDia-DKO mice, BDA-labeled corticospinal axons that arose from neurons of the motor cortex crossed the midline and projected toward the dorsal funiculus at the level of the pyramidal decussation (Fig. 3B-3D). In the spinal cord of wild-type mice, BDA-labeled axons that entered the gray matter from the dorsal funiculus were confined to the contralateral side of the BDA injection, and rarely re-crossed the midline (Fig. 3E, F). In contrast, in mDia-DKO mice, many of these axons aberrantly re-crossed the midline and projected to the gray matter of the spinal cord at the side ipsilateral to the injection side (Fig. 3G). The percent of sections showing aberrant recrossing of corticospinal axons was significantly larger in mDia-DKO mice than wild-type mice (Fig. 3H).

These data together suggest that mDia deficiency impairs axon repulsion of both spinal cord interneurons and corticospinal neurons at the midline of the spinal cord.

### **mDia is critical for axon retraction in primary cultured neurons**

To examine whether mDia is involved in EphA signaling for axon retraction, we employed primary culture of hippocampal neurons, which has been used as a model for EphA-dependent axonal retraction (Knoll *et al.* 2006). We examined effects of Ephrin-B3 that is present at the midline and prevents aberrant crossing at the spinal cord (Kullander *et al.* 2001) and those of Ephrin-A5 that similarly binds to EphA receptors and causes neurite retraction (Wahl *et al.* 2000; Cheng *et al.* 2003; Knoll *et al.* 2006). We also tested effects of semaphorin 3A (Sema-3A) that also induces axon retraction in a Rho-ROCK signaling-dependent manner (Gallo 2006). Since mDia promotes *de novo* formation of actin filaments, we stained filamentous actin with fluorescent phalloidin in

wild-type and mDia-DKO neurons without or with the stimulation. Without the stimulation, no apparent abnormality was observed in the growth cone in mDia-DKO neurons: enrichment of filamentous actin and lamellipodial formation were similarly observed in wild-type and mDia-DKO neurons (Fig. 4A). Bath application of Ephrin-B3, Ephrin-A5 or Sema3A induced growth cone collapse and axon retraction in wild-type neurons (Fig. 4A, B), as previously reported (Knoll *et al.* 2006; Iwasato *et al.* 2007; Yue *et al.* 2008). Notably, these stimuli abolished actin-rich lamellipodial and filopodial extensions, although signals for filamentous actin were maintained at the collapsed tip of the axon (Fig. 4A). On the other hand, while these stimuli induced loss of lamellipodial structure of the growth cone also in mDia-DKO neurons, they failed to induce the growth cone collapse: several actin-rich filopodial extensions remained intact (Fig. 4A, B). These findings suggest that mDia plays a role for axon retraction induced by multiple chemo-repellants through actin reorganization at the growth cone.

We then analyzed how mDia deficiency affects axon retraction by time-lapse imaging. In wild-type neurons, bath application of Ephrin-A5 immediately halted the membrane ruffling of the growth cone, and subsequently induced collapse of the growth cone followed by axon retraction (Fig. 4C-4F; Movie S2). Ephrin-A5 treatment similarly halted the membrane ruffling at the growth cone in mDia-DKO neurons, whereas growth cone collapse and axon retraction did not occur in a significant proportion (Fig. 4C-4F; Movie S3). These results show that EphA-dependent axon retraction consists of at least two processes, halting membrane ruffling with the loss of lamellipodial actin filaments at the growth cone followed by its collapse and axon retraction, and suggest that mDia functions critically in the latter process.

**mDia deficiency disrupts the midline localization of Ephrin-B3 that avoids aberrant midline crossing of axons**

It is proposed that the Ephrin-B3 is localized along the midline and this localized accumulation prevents axons from aberrant midline crossing (Kullander *et al.* 2001; Yokoyama *et al.* 2001). We therefore analyzed whether mDia deficiency could affect the midline localization of Ephrin-B3 expression by immunofluorescent staining using an antibody to Ephrin-B3 previously reported (Nakamura *et al.* 2012). Consistent with the expression of Ephrin-B3 mRNA (Kullander *et al.* 2001), Ephrin-B3 signals were observed in wild-type E14.5 embryos as a continuous band along the midline except for the region around the central canal, which was devoid of the signal (Fig. 5A). In mDia-DKO embryos, this Ephrin-B3-devoid region around the central canal expanded, and nuclear staining revealed disrupted tissue architecture in this region (Fig. 5A). Notably, axon tracer injection combined with Ephrin-B3 immunostaining revealed that most of axons aberrantly crossing the midline of mDia-DKO mice passed through the region devoid of Ephrin-B3 signals (Fig. 5B).

To examine the abnormality of tissue architecture in mDia-DKO mice further, we carried out histological analysis with H&E staining. This study revealed that neuroepithelial cell lining of the central canal was severely disorganized in mDia-DKO mice at E14.5, and that abnormal cellular dysplasia obstructed the central canal (Fig. 6A). We previously reported that loss of mDia results in disruption of neuroepithelium integrity in developing brain, leading to periventricular dysplasia (Thumkeo *et al.* 2011). We therefore suspected that a similar abnormality could occur in the developing spinal cord. Indeed, the periventricular dysplasia was found stochastically at multiple levels of the developing spinal cord, and was frequently observed as early as E9.5, which is

before the midline structure of the spinal cord is formed (Fig. 6B). Consistent with a role for mDia in neuroepithelium integrity in the spinal cord, mDia3 immunoreactivity was enriched at the apical surface of the ventricular zone in the developing spinal cord (Fig. 6C), similarly to mDia3 localization in the developing forebrain (Thumkeo et al., 2011) as well as mDia1 localization in the developing spinal cord, as previously reported (Herzog et al., 2011). These findings suggest that periventricular dysplasia develops and obstructs in the central canal and interferes with the subsequent formation of the midline structure expressing Ephrin-B3 for axon retraction in the spinal cord.

## Discussion

Here we found abnormal synchrony of the left-right limb movement during locomotion in mDia-DKO mice. Histological examination using axon tracer injection revealed aberrant midline crossing of corticospinal neurons and spinal cord interneurons, two neuronal populations involved in gait control (Asante *et al.* 2010). These findings thus illustrate critical roles of mDia in axon guidance *in vivo*.

Abnormal alternation of left-right limb movements and aberrant crossing of axons at the midline of the spinal cord observed in mDia-DKO mice were reminiscent of the phenotypes previously reported in mice lacking Ephrin-B3 or EphA4 (Kullander *et al.* 2003; Kiehn 2006). Consistent with this notion, mDia deficiency impairs axon retraction induced by EphA stimulation. Notably, mDia deficient neurons also fail to respond to Sema-3A, suggesting a role of mDia for axon retraction induced by multiple chemorepellants. Our time-lapse imaging of primary culture neurons further revealed two distinct processes of axon retraction induced by EphA stimulation: the mDia-independent halting of membrane ruffling and the mDia-dependent growth cone collapse and axon retraction. Interestingly, it was reported that pharmacological inhibition of ROCK, another Rho effector that regulates myosin activity, prevents axon retraction, but not the concomitant loss of growth cone lamellipodia, upon EphA stimulation in retinal ganglion cells (Harbott & Nobes 2005). Thus, mDia and ROCK together are involved in EphA-mediated axon retraction, but not in the loss of lamellipodia in the growth cone. Consistent with a role for mDia in actin nucleation and polymerization, our finding showed that mDia deficiency affects actin reorganization at the growth cone upon EphA stimulation. It is plausible that *de novo* synthesis of straight actin filaments is necessary for EphA-dependent growth cone collapse and axon

retraction, and actin filaments produced by the action of mDia are used for ROCK-mediated actomyosin-based contractility, leading to axon retraction. It should be noted that the action of mDia in EphA-induced axon retraction found in this study is apparently opposite to that reported in SDF-1 $\alpha$ -induced facilitation of axon elongation. Since ROCK activity suppresses mDia-mediated axon elongation by SDF-1 $\alpha$  in primary cerebellar granule cells (Arakawa *et al.* 2003), we speculate that concomitant activation of ROCK switches the mode of action of mDia from chemoattraction to chemorepulsion.

As described above, mDia deficiency abolished growth cone collapse and axon retraction, but not halting of membrane ruffling, induced by EphA stimulation. How mDia is selectively involved in one of these processes, but not the other, remains to be clarified. Since Ephexin is known to act as a guanine nucleotide factor (GEF) for Rho downstream of EphA (Shamah *et al.* 2001), Rho activated by Ephexin could activate mDia. However, simultaneous Rac inactivation is also apparently required for EphA-mediated axon retraction, because mice deficient in  $\alpha$ -chimerin, a Rac-specific GTPase activating protein activated upon Ephrin-B3-stimulation, display abnormal left-right locomotor phenotype associated with aberrant midline crossing of axons of corticospinal neurons and spinal cord interneurons (Iwasato *et al.* 2007). Furthermore, conditional deletion of Rac1 in the brain disrupts lamellipodia formation in growth cones of cerebellar granule neurons (Tahirovic *et al.* 2010). Therefore, it is likely that inactivation of Rac1 by  $\alpha$ -chimerin mediates EphA-induced loss of lamellipodial actin filaments at the growth cone, independently of mDia, which is followed by Rho-ROCK/mDia pathway to complete growth cone collapse and axon retraction.



Besides the defective axon retraction, we noted that the midline localization of Ephrin-B3 in the spinal cord was disturbed in mDia-DKO mice. This phenotype is consistent with the localization of mDia1 and mDia3 at the apical surface of the ventricular zone in the developing spinal cord (Herzog *et al.*, 2011; this study). Since mDia deficiency causes both disrupted midline localization of Ephrin-B3 and partial impairment in EphA signaling, we could not specify which of these two deficits underlies aberrant midline crossing of axons in mDia-DKO mice. However, disrupted midline localization of Ephrin-B3 could be more important than the other, because axons that aberrantly crossed the midline mostly passed the midline through the region devoid of Ephrin-B3 expression in mDia-DKO mice (see Fig. 5B). It is plausible that EphA-mediated halting of membrane ruffling at the growth cone might be sufficient to mediate the barrier function of EphrinB3 along the midline.

We previously reported that mDia deficiency disrupts the actin belt at the apical surface of neuroepithelial cells, leading to the periventricular dysplasia in the developing brain (Thumkeo *et al.* 2011). We found in this study that periventricular dysplasia similarly occurs in the spinal cord of mDia-DKO mice from E9.5, much earlier than the midline structure of the spinal cord is formed. Therefore, abnormal periventricular dysplasia could interfere with the subsequent formation of the midline structure expressing Ephrin-B3 of the spinal cord. Our finding is consistent with a recent report that genetic deletion of RhoA, a regulator for mDia, in neural progenitors causes periventricular dysplasia in the spinal cord, thereby disrupting the midline localization of Ephrin-B3 and causing aberrant midline crossing of axons of corticospinal neurons and spinal interneurons (Katayama *et al.* 2012). Therefore, the

integrity of the neuroepithelium that is maintained by the Rho-mDia pathway appears to be critical for the proper formation of the midline barrier for axon guidance.

In conclusion, our findings show that the loss of mDia impairs EphA-dependent axon retraction and disrupts the midline localization of its ligands in the spinal cord. Therefore, our study paves the way for revealing multiple roles of mDia-mediated cytoskeletal reorganization for proper axon guidance *in vivo*.

## **Experimental procedures**

### *Animals*

Wild-type C57BL/6NCrSlc mice were purchased from Japan SLC (Hamamatsu, Shizuoka, Japan). mDia1<sup>-/-</sup> mice were generated as previously described (Sakata *et al.* 2007). mDia3<sup>null</sup> (mDia3<sup>-/-</sup> or mDia3<sup>-Y</sup>) and mDia-DKO (mDia1<sup>-/-</sup>;mDia3<sup>null</sup>) mice were generated as described (Shinohara *et al.* 2012). Mutant mice used in this study were backcrossed to C57BL/6N genetic background for more than 10 generations. Genotyping of mDia1 and mDia3 deficient allele was performed as described (Sakata *et al.* 2007; Shinohara *et al.* 2012). Embryonic stages were calculated with the noon of the vaginal plug as E0.5. All animal care and use was in accordance with the *National Institutes of Health Guide for the Care and Use of Laboratory Animals* and was approved by the Institutional Animal Care and Use Committee of Kyoto University Graduate School of Medicine and Graduate School of Comprehensive Human Sciences in University of Tsukuba.

### *Analysis of gait pattern*

The gait pattern was analyzed as previously described (Kullander *et al.* 2001) . Briefly, the front or rear paws of mice were painted with blue nontoxic acrylic paint. Mice were placed at one end of a corridor of 45-cm long, 5-cm wide with 10-cm height walls on both side, and were encouraged to walk through the corridor. Seven to fourteen steps of each mouse were used for quantitative analysis of gait pattern, as described in the Results section.

### *Histological analyses*

To make embryonic and neonatal spinal cord sections, after decapitation, fresh spinal cords were rapidly dissected and immersed in 4% paraformaldehyde in 0.1 M sodium phosphate buffer (PB, pH 7.4) for overnight. For paraffin sections, the spinal cords were embedded in paraffin and cut into sections at 5-  $\mu$ m thickness. For frozen sections, the spinal cords were cryoprotected with 0.1 M PB containing 30% sucrose, and were frozen in Tissue-Tek OCT compounds (Sakura Finetek, Alphen aan den Rijn, Netherlands). Coronal sections of 30- $\mu$ m thickness were then made using the cryostat (HM500 OM, Zeiss). Hematoxylin and eosin (H&E) staining were performed using the standard protocol.

Immunostaining was performed as previously described (Kitaoka *et al.* 2007). Briefly, sections were incubated in blocking buffer (3% or 10% normal donkey serum and 0.3% Triton X-100 in phosphate-buffered saline (PBS)) for 1 h at room temperature (RT), and then with rabbit anti-Ephrin-B3 antibody (1:100, 34-3600, Life Technologies) or rabbit anti-mDia3 antibody (1: 200, Sigma) in the blocking buffer overnight at 4°C. After several washes in PBS containing 0.3% Triton X-100 (PBS-T), the sections were incubated with Alexa Fluor 488-conjugated secondary antibody (1:200 dilution, Life Technologies, Carlsbad, CA, USA) in the blocking buffer for 2 h at RT. Nuclei were counterstained with DAPI (Life Technologies) or Hoechst (Life Technologies). The spinal cord sections were mounted on MAS-coated glass slides (Matsunami, Osaka, Japan) using ProLong Gold Antifade Reagent (Life Technologies). Fluorescent images were acquired using a TCS SP5 confocal microscope (Leica Microsystems).

#### *Tracing of the corticospinal tract (CST) and the spinal-cord local circuit*

Axons projecting to the contralateral side in the spinal cord were analyzed as previously

described (Kullander *et al.* 2003). Briefly, after decapitation, fresh spinal cords were rapidly taken. A unilateral cut was made on the ventral side of the L1/L2 segment in the spinal cord of P0-P3 mice, and small crystals of rhodamine dextran amine (RDA, 3000 MW, Life Technologies) were placed in the cut. The spinal cords were incubated in oxygenated Ringers solution at RT for 5-8 h, then immersed in 4% paraformaldehyde in 0.1 M PB overnight. Sections of 30- $\mu$ m thickness were then made using the cryostat. Fluorescent images were acquired using a TCS SP5 confocal microscope (Leica Microsystems).

Anterograde tracing of CST was performed as previously described (Egea *et al.* 2005) with minor modifications. Adult mice were anesthetized with an intraperitoneal injection of ketamine (90 mg/kg) and xylazine (10 mg/kg), and biotin dextran amine (10% BDA-300 in PBS, Life Technologies) was pressure-injected to 5-7 sites in the left motor cortex through a glass pipette connected to the Pneumatic PicoPump (World Precision Instruments, Sarasota, FL, USA). The injection volume was 0.5  $\mu$ l for each injection. After postsurgical recovery for 2-3 weeks, the mice were deeply anesthetized and transcardially perfused with ice-cold PBS and 4 % paraformaldehyde in 0.1 M PB (pH 7.4). Spinal cords were removed and post-fixed, cryoprotected, and sectioned at 60- $\mu$ m thickness using the cryostat. Sections were incubated with 2% H<sub>2</sub>O<sub>2</sub> in PBS for 30 min, washed with PBS-T, and then incubated with an avidin-biotin-complex (1:100 in PBS-T, Vectastain ABC Elite Kit, Vector Laboratories, Burlingame, CA, USA) for 1 h at RT. After washing with PBS-T, the sections were rinsed with 50 mM Tris-HCl (pH 7.6) and incubated with 0.02% diaminobenzidine-4HCl (DAB) and 0.001% H<sub>2</sub>O<sub>2</sub> in 50 mM Tris-HCl (pH 7.6).

*Growth cone collapse assay*

Primary hippocampal neurons were prepared as described previously (Togashi *et al.* 2002) with minor modifications. Briefly, E17.5 embryos were taken from a pregnant mouse after cervical dislocation. Developing hippocampus was dissected from these embryos, and digested with trypsin-EDTA (Life Technologies). After trituration using fire-polished Pasteur pipette, dissociated cells were plated on glass-bottom dishes or coverslips coated with poly-L-lysine (Sigma) and laminin (Sigma) at the density of 8000-10000 cells/cm<sup>2</sup>, and cultured in Neurobasal medium (Life Technologies) supplemented with 0.5 mM L-glutamine and 2% B-27 (Life Technologies). After culture for 2 days, the neurons were stimulated for 30 min with 5 µg/ml Ephrin-A5-Fc (374-EA, R&D Systems, Minneapolis, MN, USA), 5 µg/ml Ephrin-B3-Fc (395-EB, R&D Systems), 2.5 µg/ml Sema-3A (R&D Systems, 1250-S3), or Fc (009-000-008, Jackson Immunoresearch Laboratories, West Grove, PA, USA) that had been pre-clustered with anti-Fc antibody (1/10 w/w anti-Fc/Fc; Life Technologies) for 1 h at RT. For experiments in Figures 4C-4F and Movies S2 and S3, a time-lapse, phase-contrast images of an axonal growth cone was acquired at 3-min intervals through a 20x, 0.40 N.A. objective lens attached to an inverted microscope (Leica Application Solution Multi-Dimensional Workstation, Leica Microsystems). For composite time-sequential images in Figure 4D, each of three consecutive images taken at 3-min intervals was assigned to different color channels using Photoshop CS2 (Adobe Systems).

For immunostaining for  $\beta$ III-tubulin, the neurons were fixed with 4% paraformaldehyde for 30 min, and permeabilized with 0.1% Triton X-100 in PBS for 10 min at RT. Fixed neurons were then incubated in the blocking buffer (3% normal

donkey serum in PBS) for 1 h at RT, and then with anti- $\beta$ III-tubulin antibody (1:1000, MAB1195, R&D Systems) in the blocking buffer overnight at 4°C. After several washes with PBS, they were finally incubated with Alexa Fluor 488-conjugated secondary antibody (1:200, Life Technologies), and Alexa Fluor 546-conjugated phalloidin (1:100, Life Technologies) in the blocking buffer. Fluorescent images were acquired using a TCS SP5 confocal microscope (Leica Microsystems).

#### *Statistical analyses*

All data are shown as means  $\pm$  SEM. Comparison of two groups was analyzed using unpaired two-tailed Student's *t*-test. For comparison of more than two groups, one-way or two-way ANOVA was performed and followed by Bonferroni's post hoc test for evaluation of pairwise group differences. A *P* value of less than 0.05 was considered statistically significant. The analyses were performed by Prism 4.0 software (GraphPad Software, La Jolla, CA, USA).

### **Acknowledgements**

We thank Atsushi Mizutani and Nodoka Asamoto for animal care, Tae Arai and Akiko Washimi for secretary help, and Kimiko Nonomura for technical assistance. This work was supported in part by Grant-in-Aids for Scientific Research from the Ministry of Education, Culture, Sports, Science and Technology of Japan and a CREST grant from JST. The authors declare that they have no competing interests.



## References

- Arakawa, Y., Bito, H., Furuyashiki, T., Tsuji, T., Takemoto-Kimura, S., Kimura, K., Nozaki, K., Hashimoto, N. & Narumiya, S. (2003) Control of axon elongation via an SDF-1alpha/Rho/mDia pathway in cultured cerebellar granule neurons. *J Cell Biol* **161**, 381-391.
- Asante, C.O., Chu, A., Fisher, M., Benson, L., Beg, A., Scheiffele, P. & Martin, J. (2010) Cortical control of adaptive locomotion in wild-type mice and mutant mice lacking the ephrin-Eph effector protein alpha2-chimaerin. *J Neurophysiol* **104**, 3189-3202.
- Bito, H., Furuyashiki, T., Ishihara, H., Shibasaki, Y., Ohashi, K., Mizuno, K., Maekawa, M., Ishizaki, T. & Narumiya, S. (2000) A critical role for a Rho-associated kinase, p160ROCK, in determining axon outgrowth in mammalian CNS neurons. *Neuron* **26**, 431-441.
- Chan, C.C., Khodarahmi, K., Liu, J., Sutherland, D., Oschipok, L.W., Steeves, J.D. & Tetzlaff, W. (2005) Dose-dependent beneficial and detrimental effects of ROCK inhibitor Y27632 on axonal sprouting and functional recovery after rat spinal cord injury. *Exp Neurol* **196**, 352-364.
- Cheng, Q., Sasaki, Y., Shoji, M., Sugiyama, Y., Tanaka, H., Nakayama, T., Mizuki, N., Nakamura, F., Takei, K. & Goshima, Y. (2003) Cdk5/p35 and Rho-kinase mediate ephrin-A5-induced signaling in retinal ganglion cells. *Mol Cell Neurosci* **24**, 632-645.
- Duffy, P., Schmandke, A., Sigworth, J., Narumiya, S., Cafferty, W.B. & Strittmatter, S.M. (2009) Rho-associated kinase II (ROCKII) limits axonal growth after trauma within the adult mouse spinal cord. *J Neurosci* **29**, 15266-15276.
- Egea, J., Nissen, U.V., Dufour, A., Sahin, M., Greer, P., Kullander, K., Mrcic-Flogel,

- T.D., Greenberg, M.E., Kiehn, O., Vanderhaeghen, P. & Klein, R. (2005) Regulation of EphA 4 kinase activity is required for a subset of axon guidance decisions suggesting a key role for receptor clustering in Eph function. *Neuron* **47**, 515-528.
- Fournier, A.E., Takizawa, B.T. & Strittmatter, S.M. (2003) Rho kinase inhibition enhances axonal regeneration in the injured CNS. *J Neurosci* **23**, 1416-1423.
- Gallo, G. (2006) RhoA-kinase coordinates F-actin organization and myosin II activity during semaphorin-3A-induced axon retraction. *J Cell Sci* **119**, 3413-3423.
- Hall, A. & Lalli, G. (2010) Rho and Ras GTPases in axon growth, guidance, and branching. *Cold Spring Harb Perspect Biol* **2**, a001818.
- Harbott, L.K. & Nobes, C.D. (2005) A key role for Abl family kinases in EphA receptor-mediated growth cone collapse. *Mol Cell Neurosci* **30**, 1-11.
- Herzog, D., Loetscher, P., van Hengel, J., Knüsel, S., Brakebusch, C., Taylor, V., Suter, U. & Relvas, J.B. (2011) The small GTPase RhoA is required to maintain spinal cord neuroepithelium organization and the neural stem cell pool. *J Neurosci* **31**, 5120-5130.
- Higashida, C., Miyoshi, T., Fujita, A., Ocegüera-Yanez, F., Monypenny, J., Andou, Y., Narumiya, S. & Watanabe, N. (2004) Actin polymerization-driven molecular movement of mDia1 in living cells. *Science* **303**, 2007-2010.
- Hirose, M., Ishizaki, T., Watanabe, N., Uehata, M., Kranenburg, O., Moolenaar, W.H., Matsumura, F., Maekawa, M., Bito, H. & Narumiya, S. (1998) Molecular dissection of the Rho-associated protein kinase (p160ROCK)-regulated neurite remodeling in neuroblastoma N1E-115 cells. *J Cell Biol* **141**, 1625-1636.
- Iwasato, T., Katoh, H., Nishimaru, H., Ishikawa, Y., Inoue, H., Saito, Y.M., Ando, R., Iwama, M., Takahashi, R., Negishi, M. & Itohara, S. (2007) Rac-GAP alpha-chimerin regulates motor-circuit formation as a key mediator of EphrinB3/EphA4 forward

signaling. *Cell* **130**, 742-753.

Katayama, K., Leslie, J.R., Lang, R.A., Zheng, Y. & Yoshida, Y. (2012) Left-right locomotor circuitry depends on RhoA-driven organization of the neuroepithelium in the developing spinal cord. *J Neurosci* **32**, 10396-10407.

Kiehn, O. (2006) Locomotor circuits in the mammalian spinal cord. *Annu Rev Neurosci* **29**, 279-306.

Kiehn, O. & Butt, S.J. (2003) Physiological, anatomical and genetic identification of CPG neurons in the developing mammalian spinal cord. *Prog Neurobiol* **70**, 347-361.

Kitaoka, S., Furuyashiki, T., Nishi, A., Shuto, T., Koyasu, S., Matsuoka, T., Miyasaka, M., Greengard, P. & Narumiya, S. (2007) Prostaglandin E2 acts on EP1 receptor and amplifies both dopamine D1 and D2 receptor signaling in the striatum. *J Neurosci* **27**, 12900-12907.

Knoll, B., Kretz, O., Fiedler, C., Alberti, S., Schutz, G., Frotscher, M. & Nordheim, A. (2006) Serum response factor controls neuronal circuit assembly in the hippocampus. *Nat Neurosci* **9**, 195-204.

Kolodkin, A.L. & Tessier-Lavigne, M. (2011) Mechanisms and molecules of neuronal wiring: a primer. *Cold Spring Harb Perspect Biol* **3**.

Kubo, T., Hata, K., Yamaguchi, A. & Yamashita, T. (2007) Rho-ROCK inhibitors as emerging strategies to promote nerve regeneration. *Curr Pharm Des* **13**, 2493-2499.

Kullander, K., Butt, S.J., Lebet, J.M., Lundfald, L., Restrepo, C.E., Rydstrom, A., Klein, R. & Kiehn, O. (2003) Role of EphA4 and EphrinB3 in local neuronal circuits that control walking. *Science* **299**, 1889-1892.

Kullander, K., Croll, S.D., Zimmer, M., Pan, L., McClain, J., Hughes, V., Zabski, S., DeChiara, T.M., Klein, R., Yancopoulos, G.D. & Gale, N.W. (2001) Ephrin-B3 is the

midline barrier that prevents corticospinal tract axons from recrossing, allowing for unilateral motor control. *Genes Dev* **15**, 877-888.

Nakamura, P.A., Hsieh, C.Y. & Cramer, K.S. (2012) EphB signaling regulates target innervation in the developing and deafferented auditory brainstem. *Dev Neurobiol* **72**, 1243-1255.

Narumiya, S., Tanji, M. & Ishizaki, T. (2009) Rho signaling, ROCK and mDia1, in transformation, metastasis and invasion. *Cancer Metastasis Rev* **28**, 65-76.

Ohshima, Y., Kubo, T., Koyama, R., Ueno, M., Nakagawa, M. & Yamashita, T. (2008) Regulation of axonal elongation and pathfinding from the entorhinal cortex to the dentate gyrus in the hippocampus by the chemokine stromal cell-derived factor 1 alpha. *J Neurosci* **28**, 8344-8353.

Sakata, D., Taniguchi, H., Yasuda, S., Adachi-Morishima, A., Hamazaki, Y., Nakayama, R., Miki, T., Minato, N. & Narumiya, S. (2007) Impaired T lymphocyte trafficking in mice deficient in an actin-nucleating protein, mDia1. *J Exp Med* **204**, 2031-2038.

Shamah, S.M., Lin, M.Z., Goldberg, J.L., Estrach, S., Sahin, M., Hu, L., Bazalakova, M., Neve, R.L., Corfas, G., Debant, A. & Greenberg, M.E. (2001) EphA receptors regulate growth cone dynamics through the novel guanine nucleotide exchange factor ephexin. *Cell* **105**, 233-244.

Shinohara, R., Thumkeo, D., Kamijo, H., Kaneko, N., Sawamoto, K., Watanabe, K., Takebayashi, H., Kiyonari, H., Ishizaki, T., Furuyashiki, T. & Narumiya, S. (2012) A role for mDia, a Rho-regulated actin nucleator, in tangential migration of interneuron precursors. *Nat Neurosci* **15**, 373-380, S371-372.

Swiercz, J.M., Kuner, R., Behrens, J. & Offermanns, S. (2002) Plexin-B1 directly interacts with PDZ-RhoGEF/LARG to regulate RhoA and growth cone morphology.

*Neuron* **35**, 51-63.

Tahirovic, S., Hellal, F., Neukirchen, D., Hindges, R., Garvalov, B.K., Flynn, K.C., Stradal, T.E., Chrostek-Grashoff, A., Brakebusch, C. & Bradke, F. (2010) Rac1 regulates neuronal polarization through the WAVE complex. *J Neurosci* **30**, 6930-6943.

Thumkeo, D., Shinohara, R., Watanabe, K., Takebayashi, H., Toyoda, Y., Tohyama, K., Ishizaki, T., Furuyashiki, T. & Narumiya, S. (2011) Deficiency of mDia, an Actin Nucleator, Disrupts Integrity of Neuroepithelium and Causes Periventricular Dysplasia. *PLoS One* **6**, e25465.

Togashi, H., Abe, K., Mizoguchi, A., Takaoka, K., Chisaka, O. & Takeichi, M. (2002) Cadherin regulates dendritic spine morphogenesis. *Neuron* **35**, 77-89.

Wahl, S., Barth, H., Ciossek, T., Aktories, K. & Mueller, B.K. (2000) Ephrin-A5 induces collapse of growth cones by activating Rho and Rho kinase. *J Cell Biol* **149**, 263-270.

Wegmeyer, H., Egea, J., Rabe, N., Gezelius, H., Filosa, A., Enjin, A., Varoqueaux, F., Deininger, K., Schnutgen, F., Brose, N., Klein, R., Kullander, K. & Betz, A. (2007) EphA4-dependent axon guidance is mediated by the RacGAP alpha2-chimaerin. *Neuron* **55**, 756-767.

Yokoyama, N., Romero, M.I., Cowan, C.A., Galvan, P., Helmbacher, F., Charnay, P., Parada, L.F. & Henkemeyer, M. (2001) Forward signaling mediated by ephrin-B3 prevents contralateral corticospinal axons from recrossing the spinal cord midline. *Neuron* **29**, 85-97.

Yue, X., Dreyfus, C., Kong, T.A. & Zhou, R. (2008) A subset of signal transduction pathways is required for hippocampal growth cone collapse induced by ephrin-A5. *Dev Neurobiol* **68**, 1269-1286.

### Figure legends

**Figure 1** mDia-DKO mice exhibit abnormal synchrony of left-right limb movements during locomotion. (A) Representative hindlimb footprint patterns of various mDia genotypes, such as wild-type mice, mDia1 knockout mice (mDia1<sup>-/-</sup>;mDia3<sup>+/-</sup>), mDia3 knockout mice (mDia1<sup>+/-</sup>;mDia3<sup>null</sup>), mDia3 knockout mice with mDia1 heterozygous deletion (mDia1<sup>+/-</sup>;mDia3<sup>null</sup>), and mDia-DKO mice (mDia1<sup>-/-</sup>;mDia3<sup>null</sup>). Hindlimbs were painted with ink, and the mice were placed on white paper. (B) Quantification of the degree of left-right synchrony of the hindlimb in various mDia genotypes. The ratio of the distance between adjacent footprint of left and right hindlimbs ('B') and the distance between two consecutive footprints of the same hindlimb ('A') were determined, and then the B/A ratio was compared across mDia genotypes. The number of mice is shown in each bar. The genotypes (wt, wild-type; ht, heterozygous; ko, knockout) are shown below each bar. \*\*\*  $P < 0.0001$  for a Bonferroni's *post hoc* test following one-way ANOVA.

**Figure 2** Aberrant midline crossing of axons of spinal cord interneurons in mDia-DKO mice. (A) Representative fluorescent images of RDA-labeled axons that crossed the midline in the spinal cord of wild-type and mDia-DKO mice. Crystals of RDA were applied at the L2 segment of the spinal cord of wild-type and mDia-DKO mice at P0. Photographs of the transverse sections of the L2 segment from wild-type and mDia-DKO spinal cords are shown. Regions of dashed squares in left images are magnified and shown in middle images. Commissural fibers at the most ventral region were similarly observed in wild-type and mDia-DKO spinal cords (dashed circles in middle images). Axons that aberrantly crossed the midline are highlighted by

arrowheads. Scale bar, 250  $\mu\text{m}$ . Right panels show the signal intensities of RDA along the midline (dashed lines in the middle images) in the corresponding images. RDA signals corresponding to axons that aberrantly crossed the midline in the mDia-DKO spinal cord are highlighted by a black line. Horizontal and vertical axes are shown in arbitrary units. (B) The dorso-ventral distribution of RDA signals that crossed the midline of the spinal cord in wild-type and mDia-DKO mice ( $n = 4$  and  $n = 3$ , respectively). RDA signals were scanned similarly to Fig. 2A, and were normalized to the overall average in each scanned profile. Resultant values were averaged across mice of each genotype and are shown. Horizontal and vertical axes are shown in arbitrary units. Note that the distribution of RDA signals is significantly different between the two genotypes ( $P = 0.0004$  for the Genotype  $\times$  Bin interaction in repeated-measure two-way ANOVA).

**Figure 3** Corticospinal axons aberrantly re-cross the midline of the spinal cord in mDia-DKO mice. (A) A diagram that illustrates injection sites of an anterograde tracer in the primary motor cortex (M1) and a path of the corticospinal tract (CST) axons (red line) from the cortex across the pyramidal decussation (C, D) into the spinal cord (F, G). (B) A diagram of cross-sectioned pyramidal decussation. A red line indicates a path of the labeled CST axons. (C, D) Unilateral labeled CST axons at the pyramidal decussation in wild-type (C) and mDia-DKO mice (D). The region enclosed by a dashed square in Fig. 3B is shown for each genotype. Blue and red arrows indicate CST axons before and after midline crossing, respectively. The dashed line denotes the midline. Note that CST axons form proper pyramidal decussation in both wild-type and mDia-DKO mice. (E) A diagram of cross-sectioned spinal cord. A red line indicates a

path of the labeled CST axons. (F, G) Unilateral labeled CST axons at the cervical level of the spinal cord in wild-type (F) and mDia-DKO (G). The region enclosed by a dashed square in Fig. 3E is shown for each genotype. The dashed line denotes the midline. Note that many CST axons re-crossed the midline and projected to the side ipsilateral to the tracer injection in mDia-DKO mice (black arrows). (H) Quantification of the proportion of sections with axons re-crossing the midline of the cervical spinal cord in wild-type (WT) and mDia-DKO (DKO) (9-25 sections per mice). Sections with axons re-crossing the midline were more frequently observed in mDia-DKO mice. The number of mice is shown in each bar. \*\*  $P < 0.01$  for unpaired  $t$ -test. Scale bar, 100  $\mu\text{m}$ .

**Figure 4** Axon retraction is impaired in mDia-DKO hippocampal neurons. (A) Wild-type and mDia-DKO hippocampal neurons treated with either preclustered Fc (control), Ephrin-B3-Fc or Ephrin-A5-Fc for 30 min. The treated neurons were subjected to immunostaining for  $\beta$ III-tubulin (green) and phalloidin staining (red). Scale bar, 20  $\mu\text{m}$ . (B) Quantification of the growth cone collapse induced by Ephrin-A5-Fc, Ephrin-B3-Fc and Sema-3A-Fc in wild-type (WT) and mDia-DKO (DKO) hippocampal neurons. The proportion of collapsed growth cone in neurons from each embryo was determined for statistical analyses. 474 growth cones from 6 wild-type embryos and 334 growth cones from 8 mDia-DKO embryos for Fc control; 553 growth cone from 6 wild-type embryos and 291 growth cones from 6 mDia-DKO embryos for Ephrin-A5-Fc; 435 growth cones from 3 wild-type embryos and 346 from 4 mDia-DKO embryos for Ephrin-B3-Fc; 347 growth cones from 3 wild-type embryos and 424 growth cones from 4 mDia-DKO embryos for Sema-3A-Fc. \* $P < 0.05$ ; \*\* $P < 0.01$ ; \*\*\* $P < 0.001$ ; n.s., not significant (unpaired  $t$ -test). (C) Time-lapse, phase-contrast



imaging of the growth cones of wild-type and mDia-DKO hippocampal neurons before and after bath application of preclustered Ephrin-A5-Fc (5  $\mu\text{g/ml}$ ). Phase-contrast images were acquired at 3-min intervals indicated by the number in each frame. (D) Composite time-sequential images shown in (C). Each of these images is composites of three consecutive images taken at 3-min intervals in different color channels. Immobile structure should appear in gray. (E, F) Quantification of Ephrin-A5-induced immobility of membrane ruffling and axon retraction in wild-type and mDia-DKO hippocampal neurons. The proportion of growth cones that exhibited immobility of membrane ruffling (E) or axon retraction (F) in neurons from each embryo was determined for statistical analyses. 159 neurons from 3 wild-type embryos and 116 neurons from 3 mDia-DKO embryos were examined for quantification. Two-way ANOVA showed statistical significance for the Genotype  $\times$  Treatment interaction in axon retraction ( $P < 0.001$ ). \*\*\*  $P < 0.001$ ; n. s., not significant for Bonferroni's posttests following two-way ANOVA.

**Figure 5** Disrupted midline barrier of Ephrin-B3 is associated with aberrant axon crossing of spinal cord interneurons. (A) Immunostaining for Ephrin-B3 in the spinal cord of wild-type and mDia-DKO embryos at E14.5 ( $n = 3$  for each genotype). In the merged images, Hoechst and Ephrin-B3 are shown in blue and green, respectively. Note that a midline segment devoid of Ephrin-B3 expression was broadened in mDia-DKO embryos (arrowheads). Scale bar, 250  $\mu\text{m}$ . (B) RDA axon tracing combined with Ephrin-B3 immunostaining in the spinal cord of wild-type ( $n = 4$ ) and mDia-DKO ( $n = 3$ ) embryos at P0. Arrowheads indicate axons that aberrantly cross the midline in mDia-DKO embryos. In the merged images, Hoechst, Ephrin-B3 and RDA are shown in

blue, red and green, respectively. Scale bar, 250  $\mu\text{m}$ . Rightmost panels show line-scan profiles of Ephrin-B3 and RDA signals along the midline in the corresponding images. To assess aberrant midline crossing of axons, RDA signals were measured along the line parallel to the midline and contralateral to the injection side, as illustrated by dotted lines in the adjacent left images. Horizontal and vertical axes are shown in arbitrary units.

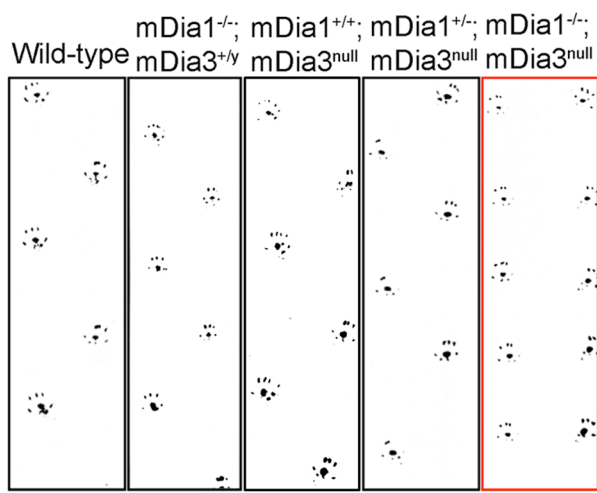
**Figure 6** Periventricular dysplasia occurs in the spinal cord of mDia-DKO neurons. (A) H&E staining in the spinal cord of wild-type and mDia-DKO embryos at E14.5 ( $n = 4$  for each genotype). Representative images of coronal sections of spinal cord are shown at lower (top) and higher (bottom) magnification. Scale bars, 250  $\mu\text{m}$  and 100  $\mu\text{m}$ , respectively. (B) Nuclear staining with Hoechst in the spinal cord of wild-type and mDia-DKO embryo at E9.5 ( $n = 3$  for each genotype). Scale bars, 100  $\mu\text{m}$ . (C) mDia3 immunostaining in the spinal cord of wild-type embryos at E13. Signals for mDia3 and nuclear staining with Hoechst are shown in green and blue, respectively. A magnified image of the apical surface is shown in insets. Note that mDia3 signals are enriched in the apical surface of the ventricular zone. Scale bar, 100  $\mu\text{m}$ .

**Movie S1** Abnormal synchrony of left and right limb movements in a representative mDia-DKO mouse.

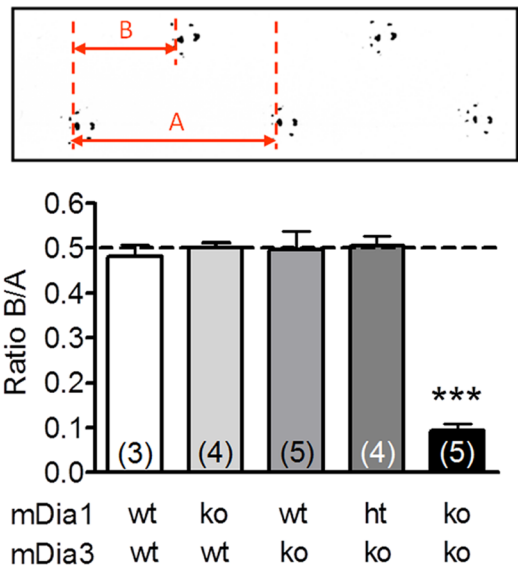
**Movie S2** Time-lapse imaging of the growth cone of a representative wild-type neuron before and after Ephrin-A5 treatment.

**Movie S3** Time-lapse imaging of the growth cone of a representative mDia-DKO neuron before and after Ephrin-A5 treatment.

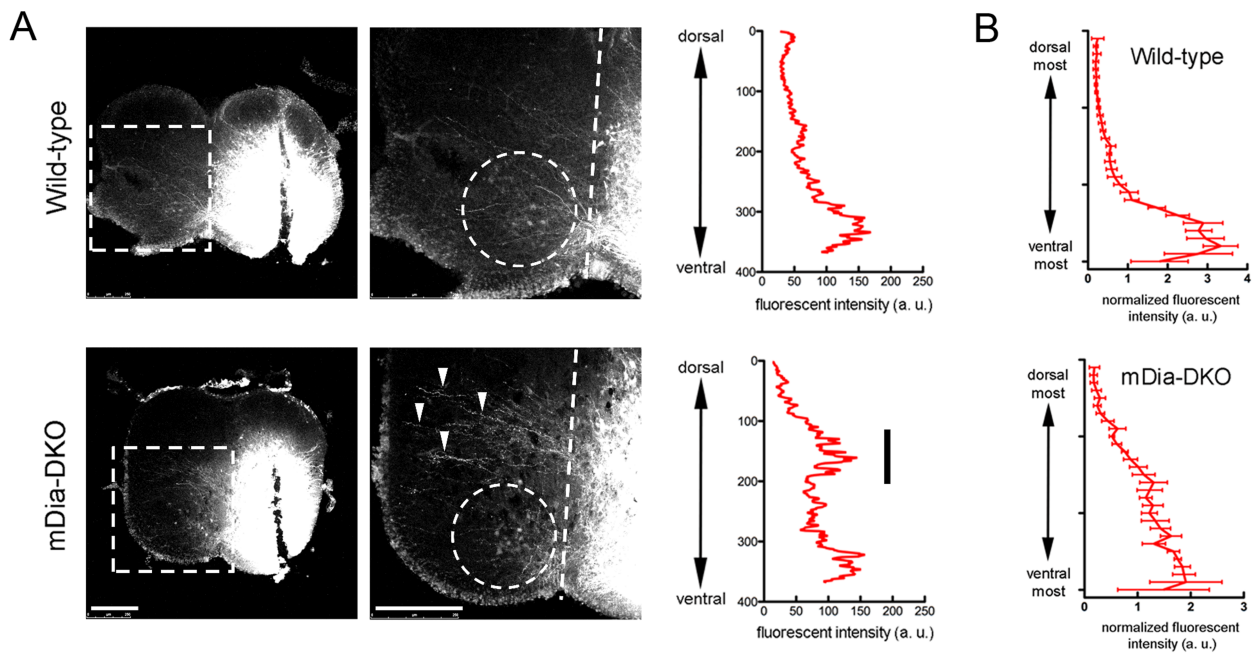
A



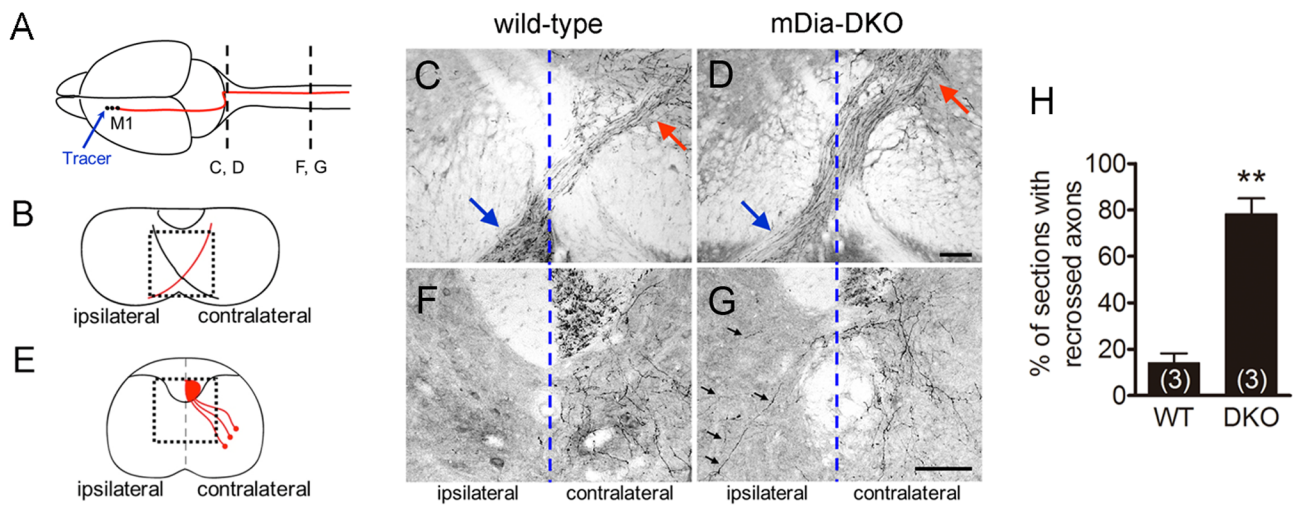
B



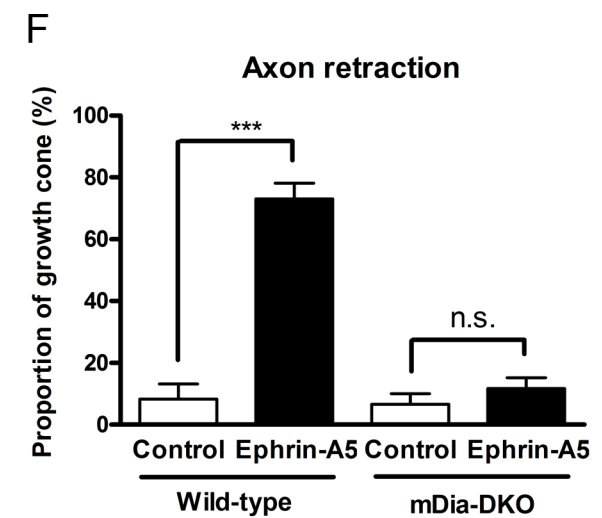
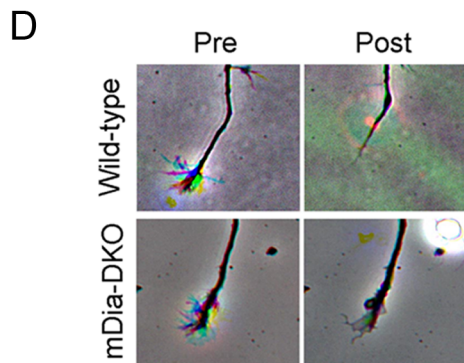
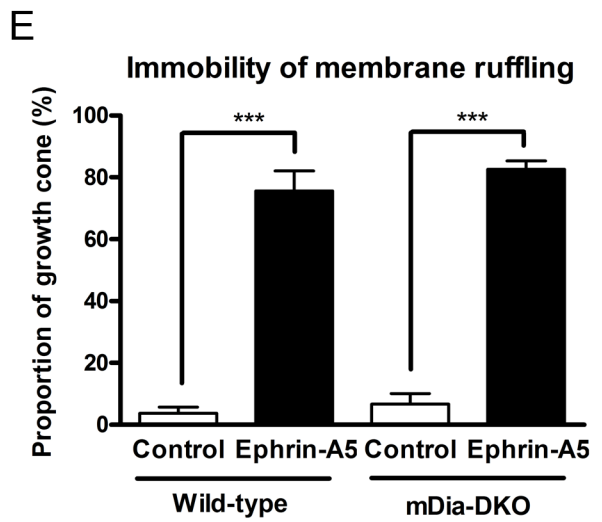
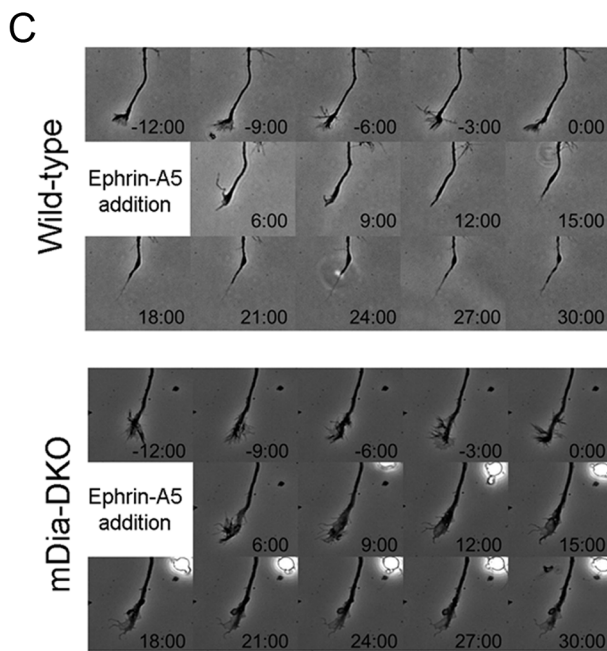
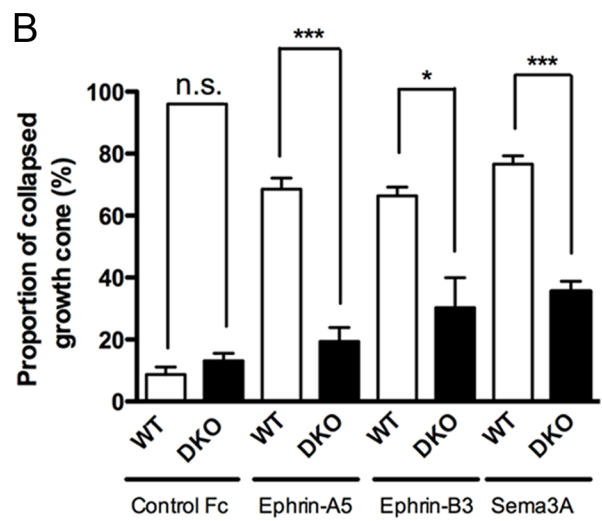
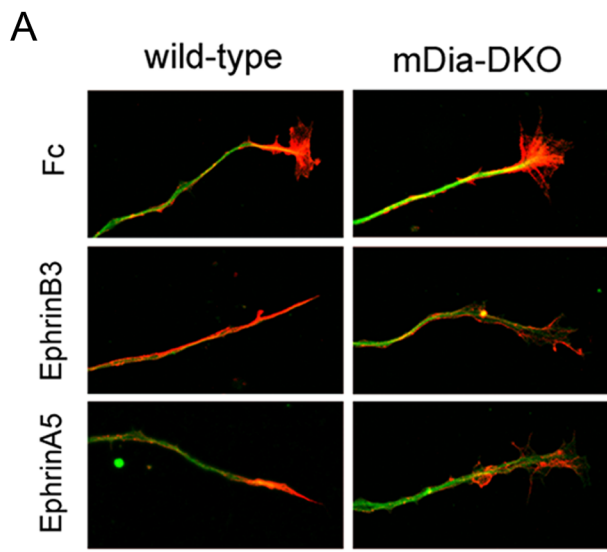
Toyoda et al., Figure 1



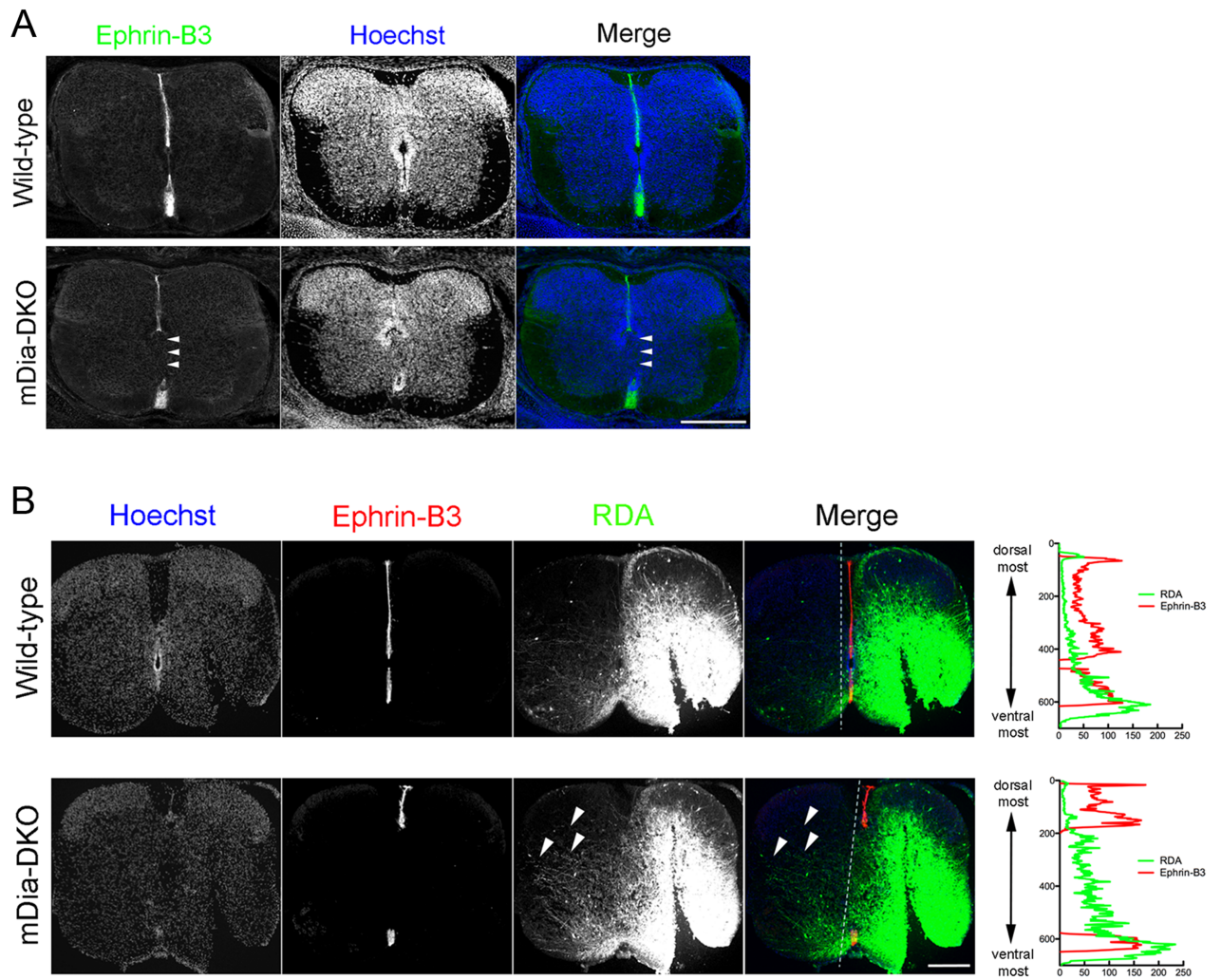
Toyoda et al., Figure 2



Toyoda et al., Figure 3

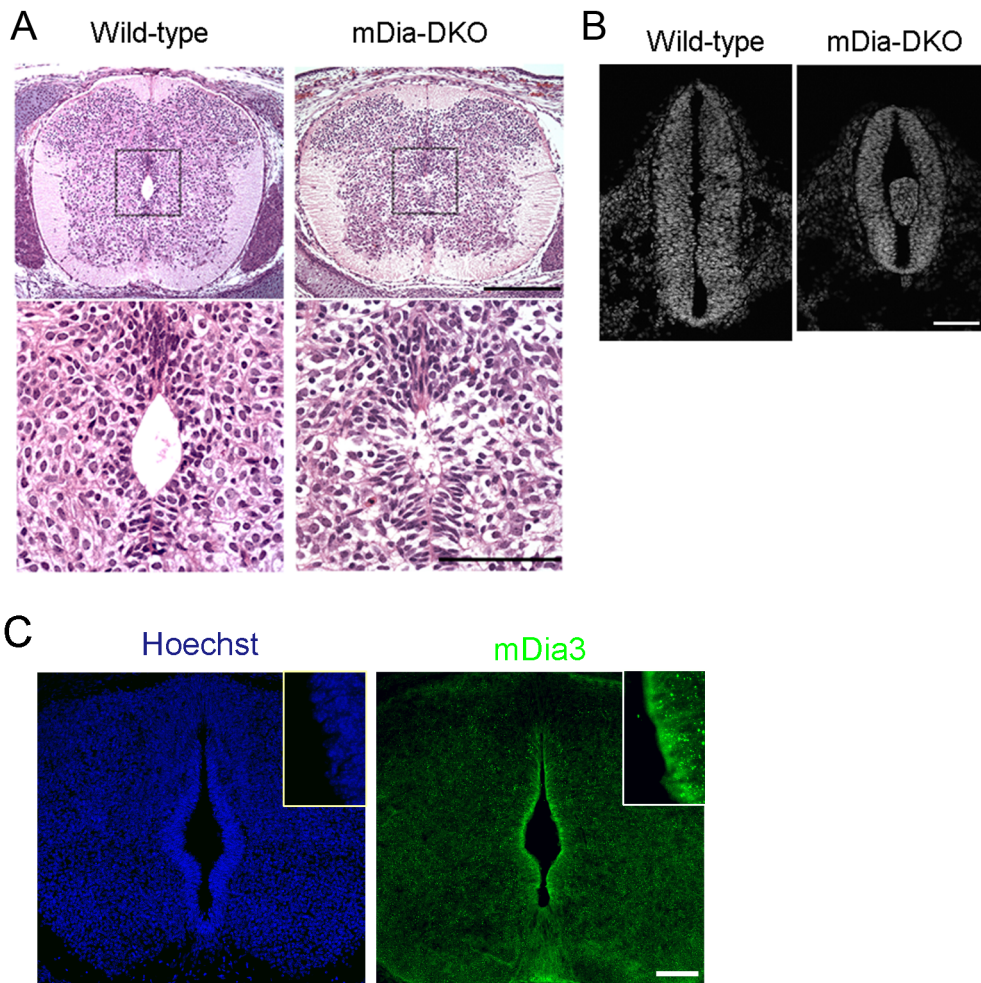


Toyoda et al., Figure 4



Toyoda et al., Figure 5





Toyoda et al., Figure 6